Supplementary Information for

Necroptosis triggers spatially restricted neutrophil-mediated vascular damage during lung ischemia reperfusion injury

Wenjun Li[1], Yuriko Terada[1], Yulia Y. Tyurina[2], Vladimir A. Tyurin[2], Amit I. Bery[3], Jason M. Gauthier[1], Ryuji Higashikubo[1], Alice Y. Tong[1], Dequan Zhou[1], Felix Nunez-Santana[4], Emilia Lecuona[4], Adil Hassan[1], Kohei Hashimoto[1], Davide Scozzi[1], Varun Puri[1], Ruben G. Nava[1], Alexander S. Krupnick[5], Kory J. Lavine[3], Andrew E. Gelman[1,6], Mark J. Miller[3], Valerian E. Kagan[2], Ankit Bharat[4], Daniel Kreisel[1,6,*]

Departments of [1]Surgery, [3]Medicine, [6]Pathology & Immunology, Washington University in St. Louis.

[2]Department of Environmental and Occupational Health, The University of Pittsburgh.

[4]Department of Surgery, Northwestern University.

[5]Department of Surgery, University of Maryland.

*Correspondence to:

Daniel Kreisel, MD PhD
email: kreiseld@wustl.edu

This PDF file includes:

Supplementary Material and Methods

Graft function assessment. Two hours after lung transplantation, mice were anesthetized, intubated and connected to the ventilator. Lungs were ventilated with a fraction of inspired oxygen of 1.0 and exposed by a sternectomy. After a 4-minute occlusion of the right hilum, arterial blood was drawn from the left ventricle. Blood gases were measured using an iSTAT Portable Clinical Analyzer (iMale STAT Corp, East Windsor, NJ).

ELISA. Serum HMGB1 levels were measured using a commercially available Enzyme-linked immunosorbent assay (ELISA) kit (IBL International) according to the manufacturer's instructions. The ELISA plate reading was performed using a Synergy HTX Multi-Mode Reader (BioTek).

Gene expression analysis. Lung tissue was digested, and single-cell suspensions were prepared as previously described (1). Cells were then stained with fluorochrome-labeled anti-CD45.2 (clone 104, BioLegend), anti-CD45.1 (clone A20, Biolegend), anti-MHC class II (clone M5/114.15.2, BD Biosciences), anti CD11b (clone M1/70, BioLegend), anti-Siglec F (clone 50-2440, BD Biosciences), anti-CD64 (clone X54-5/7.1, BioLegend), anti-Ly6G (clone 1A8, Biolegend), and anti-Ly6C (clone HK1.4, BioLegend). $CD45.2^{+}CD45.1^{-}$ $Ly6G^{-}SiglecF^{-}CD64^{-}CD11b^{+}$ $Ly6C^{low}MHCII^{-}$ non-classical monocytes were sorted flow cytometrically (FACSMelody™ (BD Biosciences)) from lungs of naïve B6 $CD45.2^{+}$ mice and B6 $CD45.2^{+}$ RIPK3-deficient mice as well as B6 $CD45.2^{+}$ RIPK3-deficient and B6 $CD45.2^{+}$ lung grafts 2 hours after transplantation into B6 $CD45.1^{+}$ hosts, as previously described (2). RNA was purified using a RNeasy mini kit (Qiagen) based on the manufacturer's protocol. RNA concentration was measured using a nanodrop spectrophotometer (ThermoFisher Scientific). Complementary DNA was synthesized using the iScript cDNA synthesis Kit (Bio-Rad) and

amplified using the SsoAdvanced PreAmp Supermix (Bio-Rad). Amplified DNA was subjected to quantitative PCR (qPCR) using the iTaq Universal SYBR Green Master Mix (Bio-Rad). Real-time qPCR was performed under the following conditions using a CFX-Connect™ (Bio-Rad): 1 cycle at 95°C for 3 minutes, then 40 cycles at 95°C for 10 seconds, 55°C for 15 seconds, and 68°C for 20 seconds, followed by 95°C for 10 seconds. The Ct values were normalized to the endogenous control (18s RNA). Primer sequences of CXCL1 were as follows: 5′-CTGGGATTCACCTCAAGAACATC-3′ (forward)/5′- CAGGGTCAAGGCAAGCCTC-3′ (reverse).

Two-photon microscopy. Lungs of naïve mice or transplant recipients as well as explanted lung tissue, in select experiments sliced with a vibratome blade, were imaged by intravital two-photon microscopy, for periods up to two hours, as previously described (3). For imaging of explanted tissue, lungs were placed in a chamber that was superfused with oxygenated (95% O2 / 5% CO2) Roswell Park Memorial Institute (RPMI) 1640 medium containing 1% penicillin/streptomycin, 25 mM Hepes and 5 g/liter glucose. For intravital imaging, mice were anesthetized with an intraperitoneal injection of ketamine (80 mg/kg) and xylazine (10 mg/kg) and intubated orotracheally with a 20 G angiocatheter which was connected to a rodent ventilator. Mice were ventilated with room air at a rate of 120 breaths per minute with a tidal volume of 0.5 ml, as described by our group and others (4-6). Mice were placed in a lateral decubitus position, lungs were exposed through a small left thoracic window between the 3rd and 7th ribs and imaged with a custom two-photon microscope using ImageWarp or SlideBook acquisition software (A&B Software: Intelligent Imaging Innovations). 15μL of 655-nm nontargeted Q-dots, suspended in 60 μl of phosphate-buffered saline were injected intravenously to label blood vessels. For select experiments, mice were treated with anti-CXCL1 or control Ig antibodies (200 μg intraperitoneally

immediately before transplantation and immediately before imaging) and PE-conjugated anti-Ly6G antibodies (2 μg, clone 1A8, ebioscience) were injected intravenously 15 minutes prior to imaging to label neutrophils. For time-lapse imaging we averaged 22 video-rate frames (0.75 seconds per slice) during the acquisition. Each plane represents an image of 220 × 240 μm in the x and y dimensions. For intravital imaging, up to 41 sequential planes and for imaging of lung explants up to 81 sequential planes were acquired in the z dimension (2.5 μm each) to form a z stack for intravital imaging. Percentages of extravasated cells were measured as previously described by our group and others (1, 2, 7-9) and as presented in Fig. S1. Vascular leakage was determined by measuring the intensity and distribution of quantum dots outside the vessels in at least 6 randomly selected vessels per experimental condition, as previously described (10). Density of neutrophils was determined as number of cells per mm^2 area. Multidimensional rendering was done with Imaris (Bitplane), whereas manual cell tracking was performed by using velocity (Improvision). Data were transferred and plotted in Graph Pad Prism 6.0 (Sun Microsystems) for analysis and creation of the graphs.

Immunostaining. Specimens were processed for immunohistochemistry and immunofluorescent staining, as previously described (11). Rabbit polyclonal anti-Nox4 (Novus Biologicals, Littleton, CO), rabbit polyclonal anti-neutrophil elastase (Abcam, Cambridge, UK) and mouse monoclonal anti-histone H2B (Abcam, Cambridge, UK) were used as primary antibodies. Secondary antibodies included goat anti-rabbit IgG (Alexa Flour 488) and goat anti-mouse Alexa Fluor 555 (Thermo Fisher Scientific, Waltham, MA) for immunofluorescence and Horse Radish Peroxidase (HRP) horse anti-rabbit IgG polymer detection kit, peroxidase and double staining Horse Radish Peroxidase (HRP) / Alkaline Phosphatase (AP) polymer kit (Vector Laboratories, Burlingame,

CA) for immunohistochemistry. Mounting medium with DAPI was used for immunofluorescence (Vector Laboratories, Burlingame, CA).

Analysis of oxygenated phosphatidylethanolamine and phosphatidylcholine by reverse phase liquid chromatography / mass spectrometry (LC/MS). Total lipids were separated on a C30 reverse phase column (Accucore, 2.1mm x 25 cm, 2.6 micron particle size, Thermo Fisher Scientific). Solvent A: Acetonitrile/water(50/50); Solvent B: 2-Propanol/acetonitile/water (85/10/5). Both A and B solvents contained 5mM ammonium formate and 0.1% formic acid as modifiers. Gradient method was as follows: 0-20 min, 30%-70% B (curvilinear, 9); 20-55 min, 70-100% B (curvilinear,9); 55-70 min, hold at 100% B; 70-85 min, 100-30% B (linear); 85-95 min, 30% B for equilibration. The flow was maintained at 100 μl/min. The liquid chromatography system was a Thermo Ultimate 3000 complete with a WPS-3000 autosampler. Column temperature was set at 35 deg. C. Mass spectrometry (MS) and tandem mass spectrometry (MS/MS) analysis of phospholipids was performed on a Q-Exactive mass spectrometer (Thermo, Inc.). Analysis was in negative ion mode at a resolution of 140,000 for the full MS scan and 17,500 for the tandem mass spectrometry scan in a data-dependent mode. The scan range for mass spectrometry analysis was 150-1800 *m/z* with a maximum injection time of 128 ms using 1 microscan and an automatic gain control target of 2×10^4. A maximum injection time of 500 ms was used for tandem mass spectrometry (high energy collisional dissociation) analysis with collision energy set to 24. An isolation window of 1.0 Da was set for the tandem mass spectrometry scans. Capillary spray voltage was set at 4.0 kV, and capillary temperature was 300 ^{O}C. Sheath and auxiliary gasses were set to 8 and 0, respectively. Analysis of data was performed by using Xcalibur operating system (ThermoFisher Scientific).

Statistics. Data were analyzed by Prism version 7.0d. For the comparison of 2 groups, data were analyzed with the Mann-Whitney *U* test. For multiple group comparisons, we tested for normality (Shapiro-Wilks test) and data were analyzed by 1-way ANOVA with post hoc Holm-Šídák test. A *P* value of less than 0.05 was considered significant.

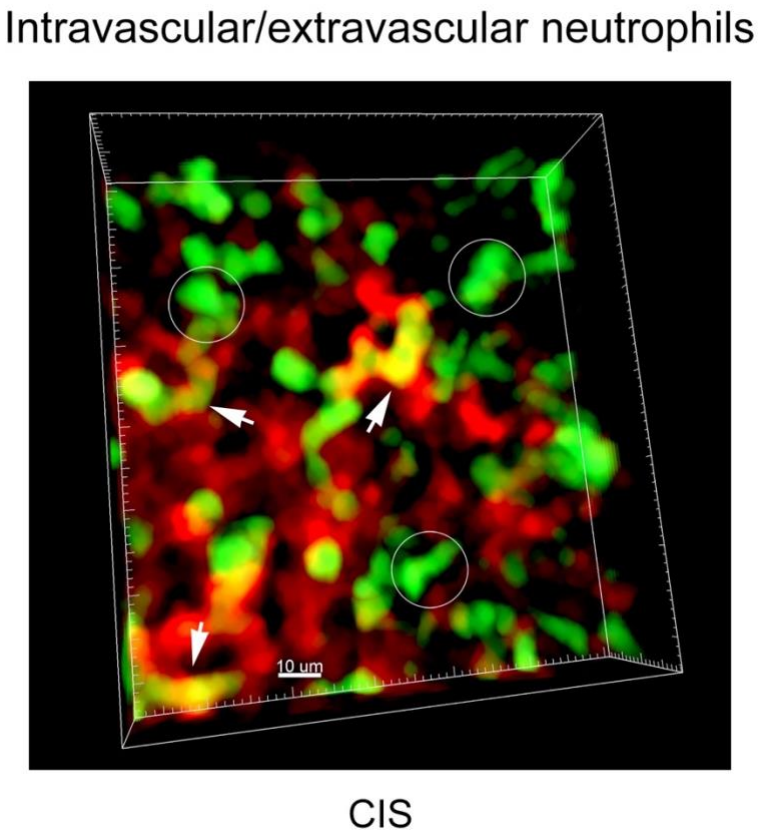

Fig. S1. Two-photon image of intravascular (green, arrow) and extravasated neutrophils (green, circled) in CIS grafts. Intravascular neutrophils overlay with vessels (labeled red after intravenous injection of quantum dots). Scale bar 10 μm.

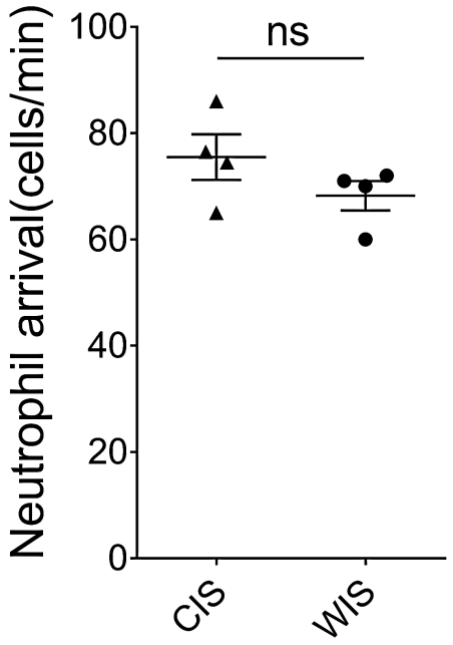

Fig. S2. Neutrophils arrive at comparable rates in lung grafts following cold or warm ischemic storage. Number of neutrophils arriving in pulmonary arterioles of CIS vs. WIS grafts per minute. Data represent the mean ± SEM (n=4). ns = not significant.

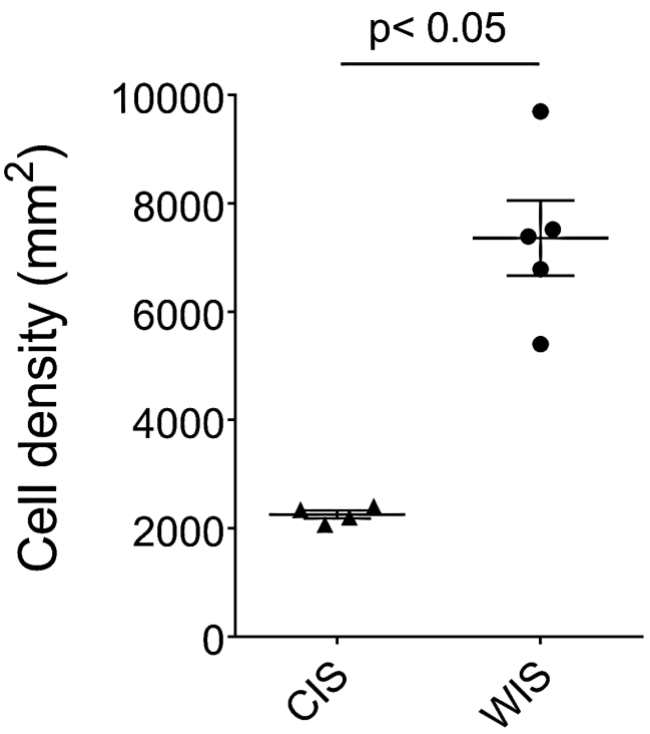

Fig. S3. Neutrophil density is increased in subpleural area in WIS compared to CIS grafts.

Neutrophil density was determined in 4-5 animals per group with 3-4 areas evaluated per animal. Data represent mean ± S.E.M.

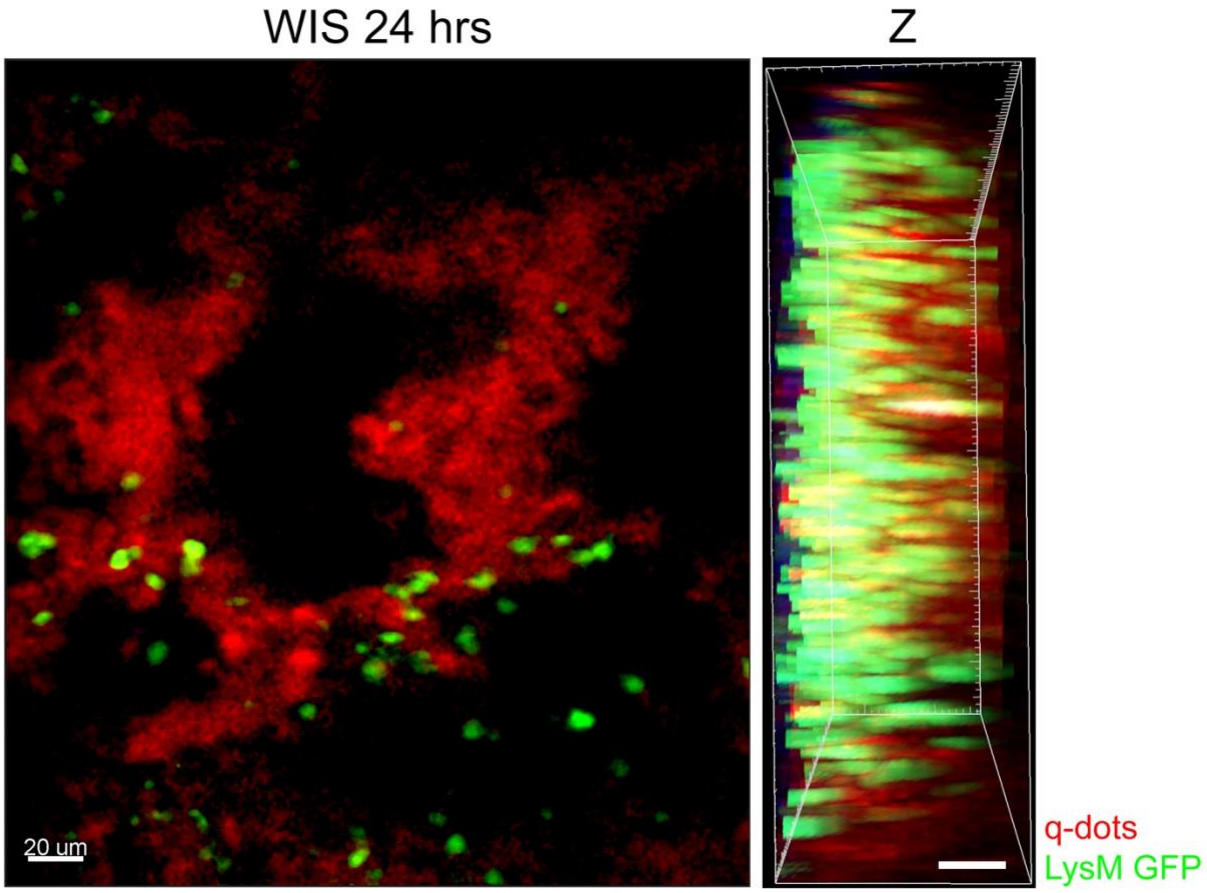

Fig. S4. Neutrophils accumulate in deeper areas of the transplanted lung at later time points after reperfusion. Two-photon image depicting neutrophils (green) in interior perialveolar capillaries (labeled red after injection of quantum dots) 24 hours after transplantation of B6 lungs into B6 LysM-GFP recipient, here shown at a depth of 60 μm (left) and side projection of z stacks (right) (scale bars: 20 μm). Left side of z stack denotes pleural surface. Images are representative of 2 independent experiments with comparable results.

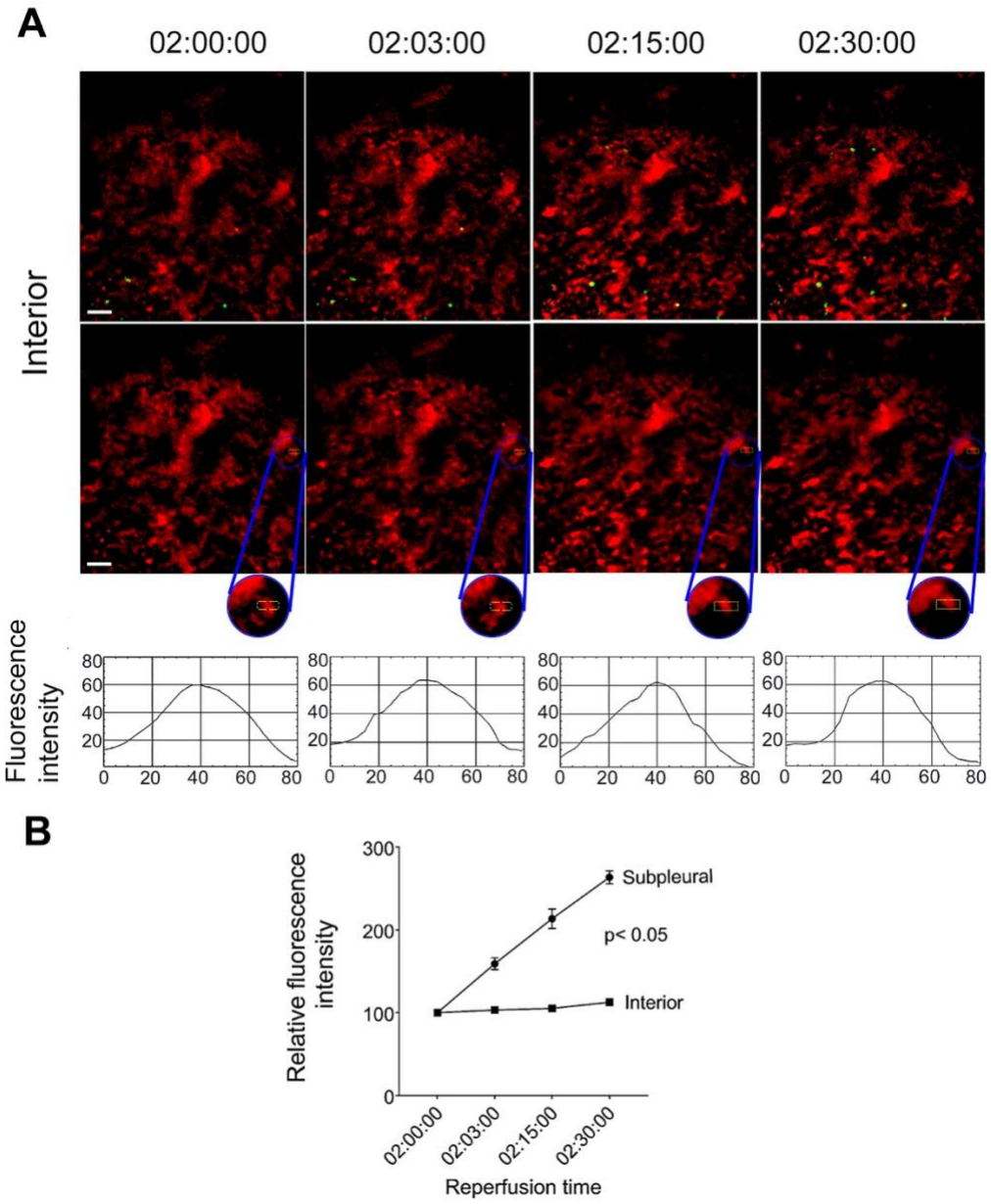

Fig. S5. Severe ischemia reperfusion injury predominantly disrupts the integrity of subpleural capillaries. A) Time lapse intravital two-photon imaging of neutrophils (green) (top panel), quantum dots (red) that were injected intravenously (middle panel) and quantification of disruption of vascular integrity in interior perialveolar capillaries as evidenced by extravascular quantum dot signal (boxed region and kymographs, bottom panel) of WIS wildtype lungs after

transplantation into syngeneic recipients. Scale bars: 30 μm. B) Comparison of extravascular quantum dot intensity around subpleural and interior perialveolar capillaries of B6 wildtype (WIS) lungs over time after transplantation into syngeneic recipients (n=4). Statistical analysis for (**B**) is for last time point.

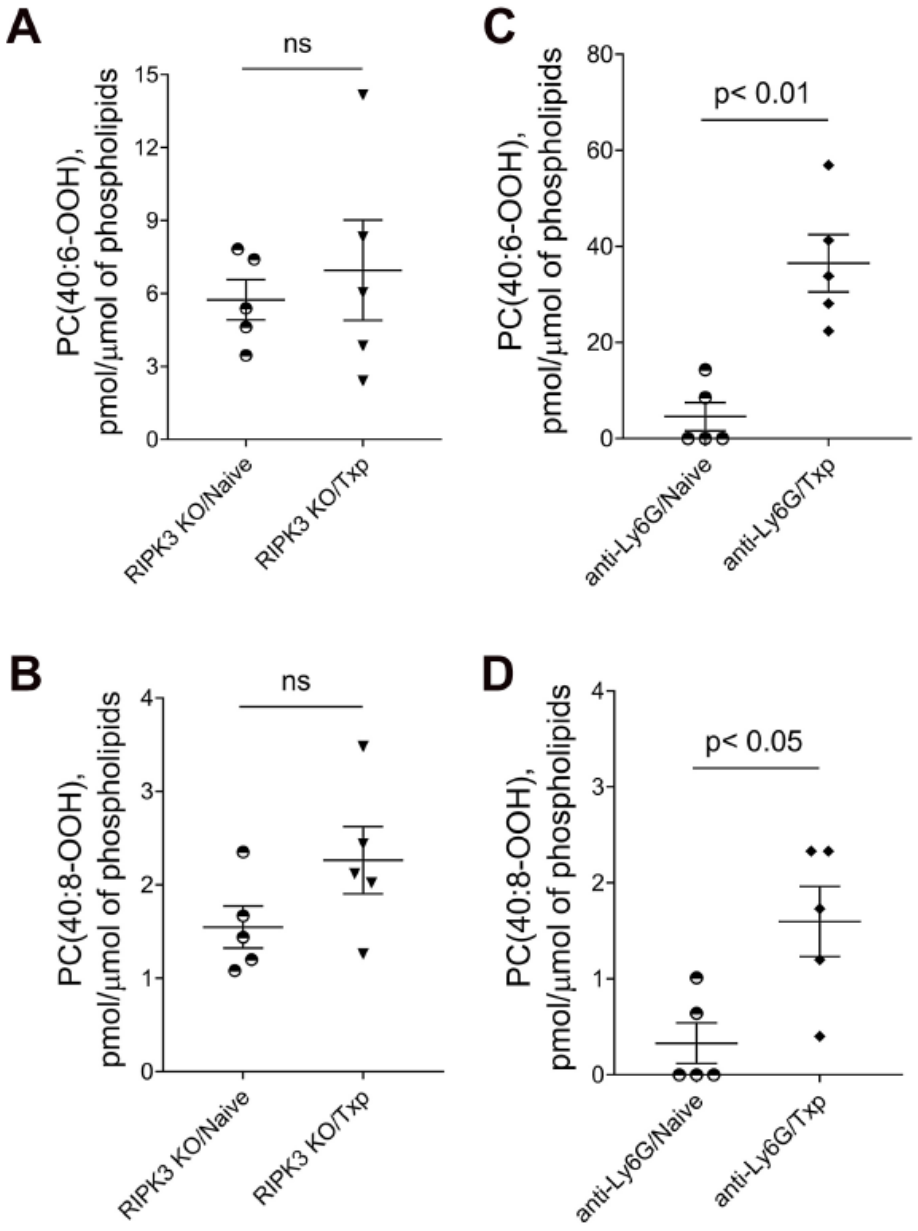

Fig. S6: Oxidized phosphatidylcholine levels are not elevated in RIP3-deficient lungs after transplantation. Graft levels of oxidized phosphatidylcholine species in A), B) naïve B6 RIPK3-deficient lungs and B6 RIP3-deficient grafts 2 hours after transplantation into B6 mice as well as in C), D) lungs of anti-Ly6G antibody-treated naïve B6 mice and B6 lungs 2 hours after transplantation into anti-Ly6G antibody-treated B6 recipients (WIS). N=5 each. Txp denotes transplantation; ns: not significant.

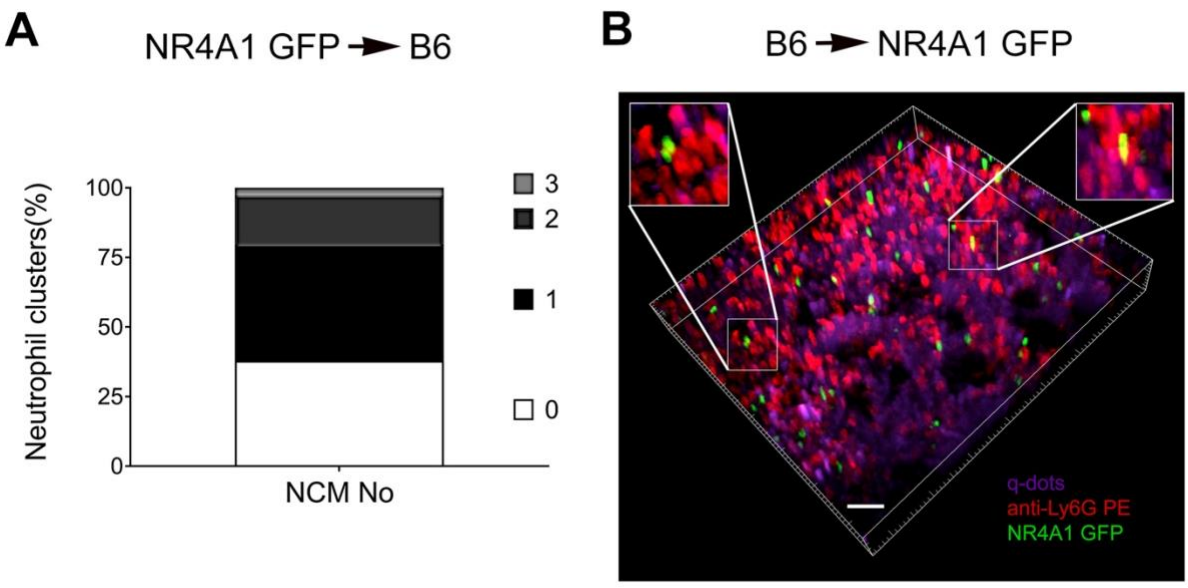

Fig. S7. Non-classical monocytes are associated with intravascular neutrophil aggregates after reperfusion of lung grafts. A) Percentage of intravascular neutrophil clusters that are associated with 0, 1, 2 or 3 donor non-classical monocytes (NCM) 2 hours after transplantation of B6 Nr4a1-GFP lungs into B6 recipients (WIS) (neutrophils were labeled red after intravenous injection of PE-labeled anti-Ly6G antibodies). B) Intravascular neutrophil clusters (red) are closely associated with recipient graft-infiltrating non-classical monocytes (green) 2 hours after transplantation of B6 lungs into B6 Nr4a1-GFP recipients. Vessels were labeled with quantum dots (purple). Images are representative of two independent experiments with comparable results. Neutrophil clusters for A) were defined as aggregates with ≥10 cells. 74 neutrophils were analyzed in 3 independent experiments. Scale bar 20 μm.

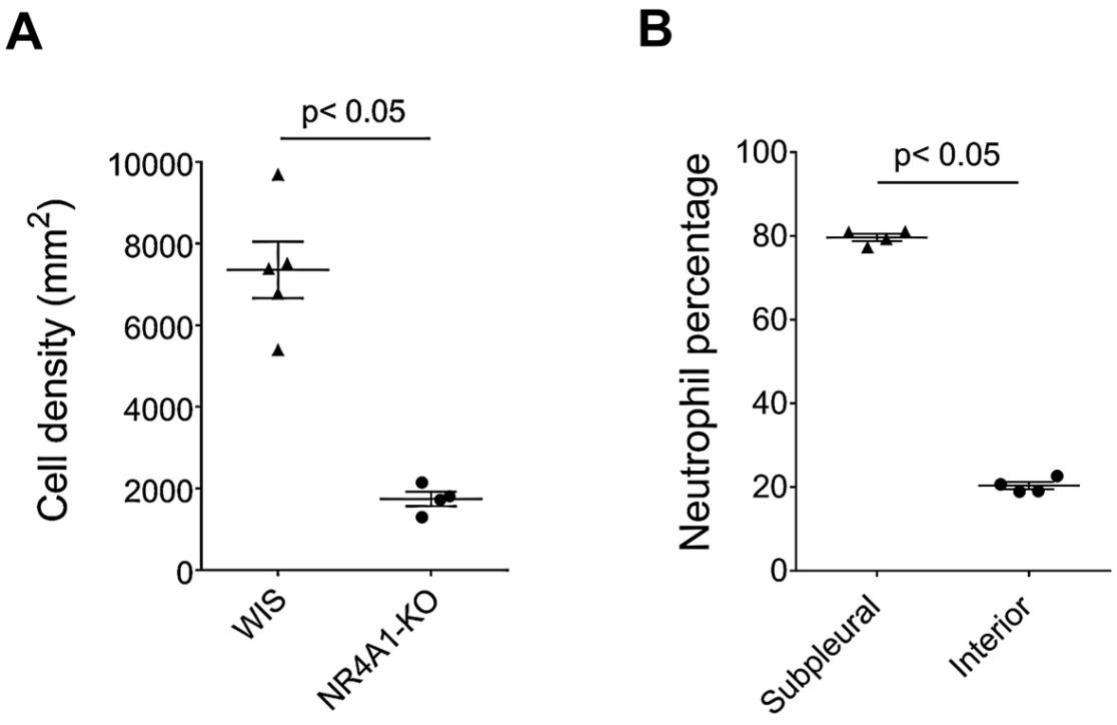

Fig. S8. Neutrophil density and distribution 2 hours after transplantation of B6 Nr4a1-deficient lungs into B6 recipients. A) Neutrophil density is decreased in subpleural area after transplantation of Nr4a1-deficient (NR4A1-KO) WIS compared to wildtype WIS grafts. Neutrophil density was determined in 4-5 animals per group with 3-4 areas evaluated per animal. B) Percentage of neutrophils in subpleural vs. interior perialveolar capillaries of Nr4a1-deficient WIS grafts. Data represent mean ± S.E.M.

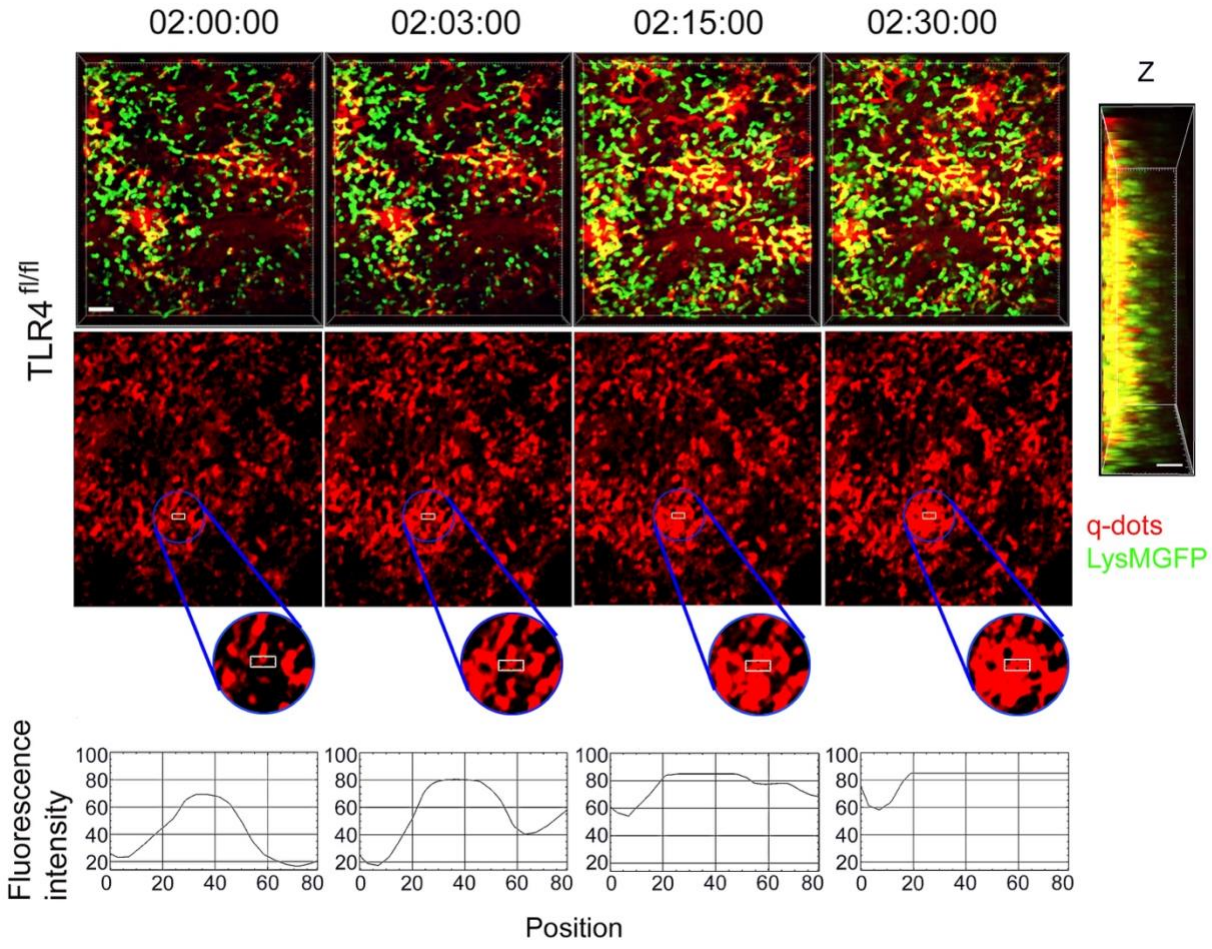

Fig. S9: Neutrophil infiltration and vascular damage in TLR4$^{fl/fl}$ lung grafts. Time lapse intravital two-photon imaging of neutrophils (green) (top), quantum dots (red) that were injected intravenously (middle) (scale bars: 30 μm), quantification of disruption of vascular integrity as evidenced by extravascular quantum dot signal (bottom, boxed region and kymographs) of TLR4$^{fl/fl}$ (WIS) lungs after transplantation into syngeneic recipients and side projection of z stacks (scale bar 20 μm). Left side of z stack denotes pleural surface.

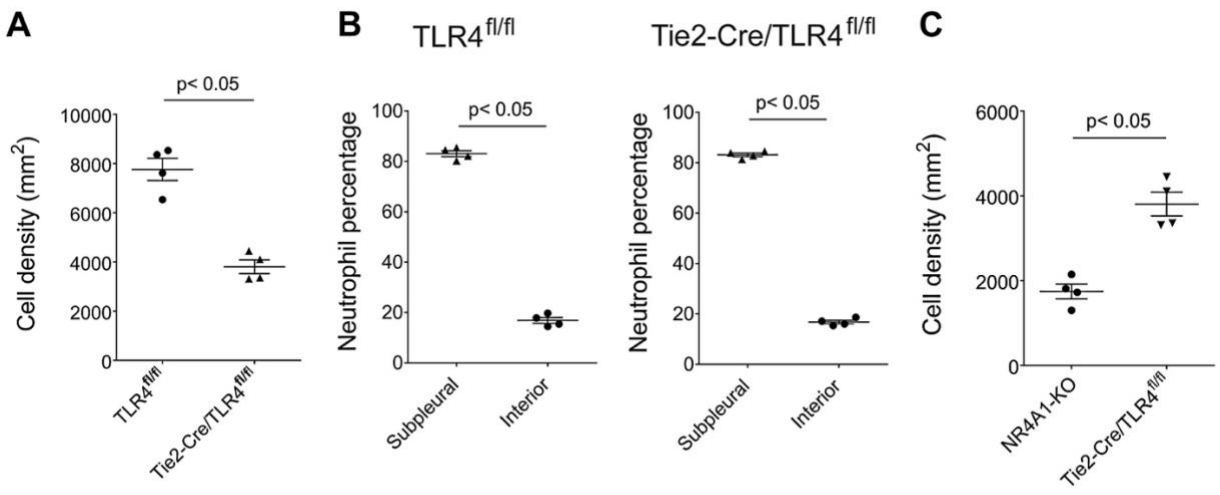

Fig. S10. Neutrophil density and distribution 2 hours after transplantation of B6 Tie2-Cre;TLR4$^{fl/fl}$ lungs into B6 recipients. A) Neutrophil density is decreased in subpleural area after transplantation of Tie2-Cre;TLR4$^{fl/fl}$ WIS compared to TLR4$^{fl/fl}$ WIS grafts. B) Percentage of neutrophils in subpleural vs. interior perialveolar capillaries of TLR4$^{fl/fl}$ and Tie2-Cre;TLR4$^{fl/fl}$ WIS grafts. C) Neutrophil density is decreased in subpleural area after transplantation of Nr4a1-deficient WIS compared to Tie2-Cre;TLR4$^{fl/fl}$ WIS grafts. Neutrophil density was determined in 4-5 animals per group with 3-4 areas evaluated per animal. Data represent mean ± S.E.M.

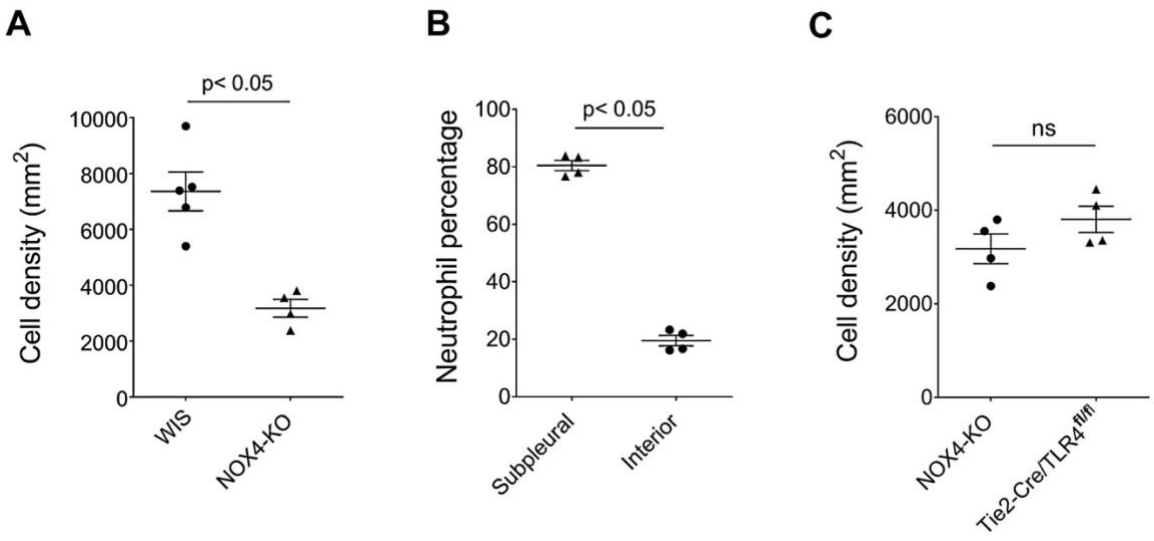

Fig. S11. Neutrophil density and distribution 2 hours after transplantation of B6 NOX4-deficient lungs into B6 recipients. A) Neutrophil density is decreased in subpleural area after transplantation of NOX4-deficient (NOX4-KO) WIS compared to wildtype WIS grafts. Neutrophil density was determined in 4-5 animals per group with 3-4 areas evaluated per animal. B) Percentage of neutrophils in subpleural vs. interior perialveolar capillaries of NOX4-deficient WIS grafts. C) Neutrophil density in subpleural area after transplantation of NOX4-deficient WIS compared to Tie2-Cre;TLR4$^{fl/fl}$ WIS grafts. Data represent mean ± S.E.M. ns = not significant.

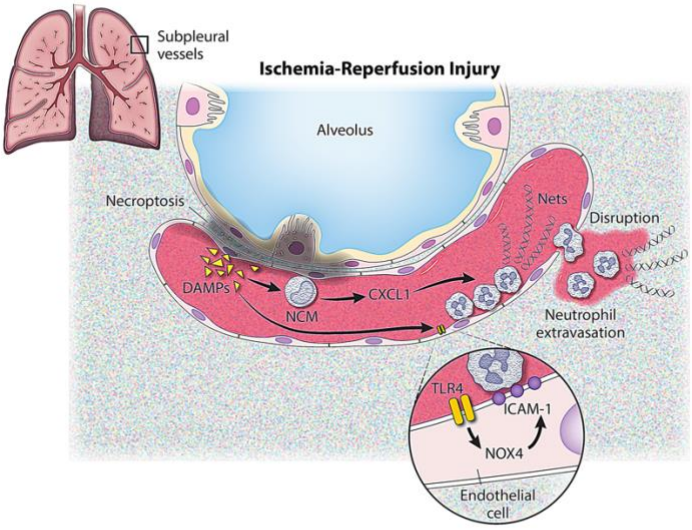

Fig. S12. Schematic diagram depicting neutrophil recruitment to injured lungs.

Movie S1. Time-lapse intravital two-photon imaging of neutrophil behavior in lungs of naïve B6 LysM-GFP mice. Neutrophils (green with red ring after intravenous injection of PE-conjugated anti-Ly6G antibodies) travel through subpleural capillaries. Blood vessels (purple) were labeled by intravenous injection of nontargeted 655nm quantum dots. Scale bar: 20 μm. Relative time is displayed in hrs:min:sec.

Movie S2. Time-lapse intravital two-photon imaging of neutrophil behavior in B6 lungs (CIS) two hours after transplantation into B6 LysM-GFP recipients. Neutrophils (green) are seen moving through subpleural capillaries with few arresting and extravasating. Blood vessels (red) were labeled by intravenous injection of nontargeted 655nm quantum dots. Scale bar: 30 μm. Relative time is displayed in hrs:min:sec.

Movie S3. Time-lapse intravital two-photon imaging of neutrophil behavior in B6 lungs (WIS) two hours after transplantation into B6 LysM-GFP recipients. Many neutrophils (green) adhere to vessel walls in capillaries, extravasate and form large clusters. Blood vessels (red) were labeled by intravenous injection of nontargeted 655nm quantum dots. Scale bar: 30 μm. Relative time is displayed in hrs:min:sec.

Movie S4. Time-lapse intravital two-photon imaging of B6 lungs (WIS) two hours after transplantation into B6 LysM-GFP recipients that were treated with neutrophil-depleting antibodies. Markedly fewer neutrophils (green) are observed after treatment with anti-Ly6G antibodies when compared to control WIS grafts (Movie S3). Blood vessels (red) were labeled by intravenous injection of nontargeted 655nm quantum dots. Scale bar: 30 μm. Relative time is displayed in hrs:min:sec.

Movie S5. Time-lapse intravital two-photon imaging of B6 lungs (WIS) two hours after transplantation into B6 LysM-GFP recipients that were treated with Nec-1. Many neutrophils (green) remain motile in the subpleural capillaries and fewer neutrophils extravasate when compared

to control WIS grafts (Movie S3). Blood vessels (red) were labeled by intravenous injection of nontargeted 655nm quantum dots. Scale bar: 30 μm. Relative time is displayed in hrs:min:sec.

Movie S6. Time-lapse intravital two-photon imaging of B6 Ripk3-deficient lungs (WIS) two hours after transplantation into B6 LysM-GFP recipients. Neutrophil (green) trafficking behavior in Ripk3-deficient lung grafts is comparable to that observed after treatment with Nec-1 (Movie S5). Blood vessels (red) were labeled by intravenous injection of nontargeted 655nm.

Movie S7. Time-lapse intravital two-photon imaging of B6 Nr4a1-deficient lungs (WIS) two hours after transplantation into B6 LysM-GFP recipients. Neutrophil (green) trafficking behavior in Nr4a1-deficient lung grafts is comparable to that observed in Ripk3-deficient grafts (Movie S6). Blood vessels (red) were labeled by intravenous injection of nontargeted 655nm quantum dots. Scale bar: 30 μm. Relative time is displayed in hrs:min:sec.

Movie S8. Time-lapse intravital two-photon imaging of B6 TLR4-deficient lungs (WIS) two hours after transplantation into B6 LysM-GFP recipients. Many neutrophils (green) remain motile in the subpleural capillaries, only few neutrophils extravasate and the formation of large neutrophil aggregates is not observed. Blood vessels (red) were labeled by intravenous injection of nontargeted 655nm quantum dots. Scale bar: 30 μm. Relative time is displayed in hrs:min:sec.

Movie S9. Time-lapse intravital two-photon imaging of B6 Tie2-Cre/TLR4$^{fl/fl}$ lungs (WIS) two hours after transplantation into B6 LysM-GFP recipients. Neutrophil (green) trafficking behavior in Tie2-Cre/TLR4$^{fl/fl}$ lungs is comparable to that observed in TLR4-deficient pulmonary grafts (Movie S8). Blood vessels (red) were labeled by intravenous injection of nontargeted 655nm quantum dots. Scale bar: 30 μm. Relative time is displayed in hrs:min:sec.

Movie S10. Time-lapse intravital two-photon imaging of B6 NOX4-deficient lungs (WIS) two hours after transplantation into B6 LysM-GFP recipients. Neutrophil (green) trafficking behavior in NOX4-deficient lungs is comparable to that observed in TLR4-deficient (Movie S8) and Tie2-

Cre/TLR4$^{fl/fl}$ (Movie S9) pulmonary grafts. Blood vessels (red) were labeled by intravenous injection of nontargeted 655nm quantum dots. Scale bar: 30 μm. Relative time is displayed in hrs:min:sec.

Movie S11. Time-lapse intravital two-photon imaging of B6 lungs (WIS) two hours after transplantation into B6 LysM-GFP recipients that were treated with DNAse. Only few neutrophils (green) adhere in the subpleural capillaries and few neutrophils extravasate when compared to control WIS grafts (Movie S3). Blood vessels (red) were labeled by intravenous injection of nontargeted 655nm quantum dots. Scale bar: 30 μm. Relative time is displayed in hrs:min:sec.

References

1. Hsiao HM, *et al.* (2018) Spleen-derived classical monocytes mediate lung ischemia-reperfusion injury through IL-1beta. *J Clin Invest* 128(7):2833-2847.
2. Zheng Z, *et al.* (2017) Donor pulmonary intravascular nonclassical monocytes recruit recipient neutrophils and mediate primary lung allograft dysfunction. *Sci Transl Med* 9(394).
3. Kreisel D, *et al.* (2010) In vivo two-photon imaging reveals monocyte-dependent neutrophil extravasation during pulmonary inflammation. *Proc Natl Acad Sci U S A* 107(42):18073-18078.
4. Okazaki M, *et al.* (2007) A mouse model of orthotopic vascularized aerated lung transplantation. *Am J Transplant* 7(6):1672-1679.
5. Fan L, *et al.* (2011) Neutralizing IL-17 prevents obliterative bronchiolitis in murine orthotopic lung transplantation. *Am J Transplant* 11(5):911-922.
6. Jungraithmayr WM, Korom S, Hillinger S, & Weder W (2009) A mouse model of orthotopic, single-lung transplantation. *J Thorac Cardiovasc Surg* 137(2):486-491.
7. Li W, *et al.* (2019) Ferroptotic cell death and TLR4/Trif signaling initiate neutrophil recruitment after heart transplantation. *J Clin Invest* 129(6):2293-2304.
8. Walch JM, *et al.* (2013) Cognate antigen directs CD8+ T cell migration to vascularized transplants. *J Clin Invest* 123(6):2663-2671.
9. Michael BD, *et al.* (2020) Astrocyte- and Neuron-Derived CXCL1 Drives Neutrophil Transmigration and Blood-Brain Barrier Permeability in Viral Encephalitis. *Cell Rep* 32(11):108150.
10. Cain MD, *et al.* (2017) Virus entry and replication in the brain precedes blood-brain barrier disruption during intranasal alphavirus infection. *J Neuroimmunol* 308:118-130.
11. Li W, *et al.* (2019) Bronchus-associated lymphoid tissue-resident Foxp3+ T lymphocytes prevent antibody-mediated lung rejection. *J Clin Invest* 129(2):556-568.